

Searching High Redshift Large-Scale Structures: Photometry of Four Fields Around Quasar Pairs at $z \sim 1$

N. V. Boris¹, L. Sodré Jr.¹, E. S. Cypriano², W. A. Santos¹, C. Mendes de Oliveira¹
and M. West³

ABSTRACT

We have studied the photometric properties of four fields around the high-redshift quasar pairs QP1310+0007, QP1355-0032, QP0110-0219, and QP0114-3140 at $z \sim 1$ with the aim of identifying large-scale structures- galaxy clusters or groups- around them. This sample was observed with GMOS in Gemini North and South telescopes in the g' , r' , i' , and z' bands, and our photometry is complete to a limiting magnitude of $i' \sim 24$ mag (corresponding to $\sim M_i^* + 2$ at the redshift of the pairs). Our analysis reveals that QP0110-0219 shows very strong and QP1310+0007 and QP1355-0032 show some evidence for the presence of rich galaxy clusters in direct vicinity of the pairs. On the other hand, QP0114-3140 could be an isolated pair in a poor environment. This work suggest that $z \sim 1$ quasar pairs are excellent tracers of high density environments and this same technique may be useful to find clusters at higher redshifts.

Subject headings: galaxies: clusters: general — galaxies: distances and redshifts — galaxies: high-redshift — large-scale structure of universe — quasars: general — X-ray: galaxies: clusters

1. Introduction

The study of galaxy populations in high-redshift large-scale structures can give us important clues about the star formation history and galaxy formation process in such environments (White & Frenk 1991; Bekki 1998; Kodama et al. 1998; van Dokkum 2005; Mei et al. 2006). However, the detection of distant galaxy clusters is not trivial.

¹Departamento de Astronomia, Instituto de Astronomia, Geofísica e Ciências Atmosféricas, Universidade de São Paulo, Rua do Matão 1226, Cidade Universitária 05508-900, São Paulo, SP, Brazil; natalia@astro.iag.usp.br

²Department of Physics and Astronomy, University College London, Gower Street, London, WC1E 6BT, United Kingdom

³Gemini Observatory/AURA, Southern Operations Center, Casilla 603, La Serena, Chile

At high redshifts, the use of techniques like the red-cluster sequence (Gladders & Yee 2005), is less efficient. The reason is the proportional decrease of the number of red galaxies in clusters for increasing redshift (e.g. Butcher & Oemler 1984). Therefore, in order to detect high- z clusters through optical imaging, one requires at least photometric redshift information, which implies imaging in four or more bands. Additionally, in order to avoid the high observational cost of observing large areas of the sky, one can use several indicators of the presence of high- z clusters to select the fields to be observed.

Several of these tracers, like extended X-ray emission (e.g., Romer et al. 2001), the Sunyaev-Zeldovich decrement or bright radio-emitting galaxies have been largely used to trace clustering of galaxies. These techniques have strengths and drawbacks. The first two, for example, depend on the presence of a hot intra-cluster medium, which may bias samples against recently forming clusters. In this paper, we will consider another possible tracer of the presence of clusters: physically close pairs of quasars.

Quasars are relatively rare astronomical objects and hence, if they are distributed following galaxies, the presence of two or more such objects in a relatively small volume should be a good indicator of a rich environment. Actually, in structure formation scenarios with bias between barionic and dark matter distribution (e.g., Kaiser 1984) it is expected that high redshift objects form in large high-redshift density fluctuations and, therefore, such correlation between quasar concentration and clusters is somewhat expected, unless, for some reason, quasars avoid clusters. However, most observational evidence shows that high redshift quasars do tend to follow the overall large scale structures.

Whether quasars inhabit or not high density regions in low redshifts is a subject of dispute. Coldwell et al. (2002), for example, claim that at $0.1 \leq z \leq 0.25$, quasars (both radio-loud and radio-quiet) tend to reside in low density regions. On the other hand Mullis et al. (2004), using a sample of X-ray selected quasars, conclude that those objects trace closely the underlying mass distribution. Söchting et al. (2002) also points out that $0.2 < z < 0.3$ quasars follow the large-scale structure traced by galaxy clusters, but they also note the complete absence of radio-quiet QSO's at the very center of galaxy clusters.

At higher redshift, however, most observational results suggest that quasars prefer groups or clusters (Hall & Green 1998; Wold et al. 2000, 2001). One very convincing example is the structure found by Haines et al. (2001) at $z = 1.226$ around a radio-quiet quasar belonging to a large quasar structure (Clowes & Campusano 1991, 1994). The same behaviour appears to be followed by radio-loud quasars. A good example is the work by Sánchez & González-Serrano (2002), who found a highly significant excess of galaxies around radio-loud quasars at $1.0 < z < 1.6$. Tanaka et al. (2001) also points in the same direction by reporting an overdensity of galaxies around a quasar concentration at $z \sim 1.1$. An excep-

tion is the work by Coil et al. (2007) who, through an analysis of the clustering of quasars and galaxies at $0.7 < z < 1.4$, concluded that quasars and blue galaxies are found in the same environment, which differs from that occupied by the red galaxy population. Regarding specifically quasar pairs, Zhdanov & Surdej (2001) found an statistically significant excess of high-redshift quasar pairs with separations between 1 and 5 Mpc in projected distance. This suggests that such quasar pairs belong to sizable physical structures (precursors of today’s clusters and superclusters of galaxies) and therefore, they can be used as tracers of high-redshift large-scale structures. Going to even larger redshifts, Djorgovski et al. (2003) found that a quasar pair at $z = 4.96$ is associated with a large-scale structure. Thus, an interesting form to search for high-redshift clusters and other large-scale structures is examining the environment inhabited by quasar pairs.

In this work, we describe a multi-color photometric study of the field around four quasar pairs at $z \sim 1$, using the instrument GMOS in both Gemini North and South telescopes.

One of the pairs in our sample, QP0110-0219, has been previously studied by Surdej et al. (1986), who found hints of the presence of a cluster around it. The new data we present here allow us to confirm this claim. There are no studies in the literature for the other three quasar pairs.

The outline of this paper is the following: in Section 2 we describe the sample and the data reduction procedures. The galaxy photometry is discussed in Section 3. Section 4 outlines our approach to obtain photometric redshifts and presents then application to our galaxy sample. The environments of the quasar pairs are discussed in section 5. Finally, in Section 6 we summarize our results. Throughout this paper, we adopt a Λ CDM concordance cosmology with $\Omega_m = 0.3$ and $\Omega_\Lambda = 0.7$, and we use the value $h = 0.7$ in the Hubble constant, $H_0 = 100 h \text{ km s}^{-1} \text{ Mpc}^{-1}$.

2. Observations and data reduction

2.1. Sample selection

In this paper, we study a sample of four fields around quasar pairs at $z \sim 1$. We selected the pairs from Véron-Cetty & Véron (2001) quasar catalog considering redshift differences smaller than 0.01 and projected angular separations smaller than 300 arcsec. We did not consider pairs with angular separations smaller than 15 arcsecs to avoid including gravitational lens. With these parameters, we found 84 quasar pairs. Five of them had redshifts between 0.9 and 1.0, and four were observed with Gemini telescopes. The main sample characteristics are shown in Table 1. It includes: the quasar names, their coordinates, redshifts,

angular separation, and the name adopted for the pairs in this paper.

We have checked the spectra of the quasars in our sample to certify that we indeed did not pick any cases of gravitationally lensed images of one only quasar. The parity of QP0110-0219 is discussed by Surdej et al. (1986). Considering the redshift difference and spectral characteristics, they conclude that the quasars Q 0107-0235 and PB 6291 are different objects. For the other pairs, quasar spectra are available in the 2dF QSO Redshift Survey (Croom et al. 2004)¹. Our visual examination of the spectra indicates that also in this case the differences in redshifts and spectral characteristics suggest that they are indeed different objects and not lensed images of the same quasar. Moreover, in QP1310+0007, QP1355-0032, and QP0110-0219 one of the quasars is radio-loud and the other is radio-quiet. Consequently, we are confident that none of the pairs in our sample are produced by gravitational lensing.

2.2. Imaging and data reduction

The four fields in Table 1 were observed with GMOS N and S mounted on Gemini telescopes. The imaging was done in four filters of the SDSS system (Fukugita et al. 1996): g' , r' , i' , and z' . The log of observations is presented in Table 2, which shows the telescope used, the exposure time, and the Gemini program identification number. All observations were performed in photometric conditions. The typical FWHM for point sources was ~ 0.7 arcsec in all images.

Data reduction was performed using the Gemini IRAF ² package. The images were bias corrected, flat fielded, and fringe corrected in the standard way. After that, they were combined and cleaned of cosmic ray events and bad pixels producing, then, the final images, appropriate for science analysis.

3. Photometry and object detection

We have used the IRAF package *daophot* to calculate the photometric zero-point for each band in each field in the AB SDSS photometric system. The calibration was made

¹http://www.2dfquasar.org/Spec_Cat/2qzsearch2.html

²IRAF is distributed by the National Optical Astronomy Observatories, which are operated by the Association of Universities for Research in Astronomy, Inc., under cooperative agreement with the National Science Foundation.

using stars from the Landolt catalog (Landolt 1992) also calibrated in the AB SDSS system. Using the dispersion in the magnitudes of the stars, we have estimated the accuracy of the magnitude zero-point as 0.01 in g' and r' bands, 0.02 in i' band, and 0.03 in z' band.

We have used SExtractor (Bertin & Arnouts 1996) to detect objects over the final image frames. First, we ran the program on the images of each photometric band and selected the image that showed the highest number of detected objects. Second, using such image as reference, we ran the program again in "dual image mode". We used a top-hat filter and detected objects above 1.5σ , which corresponded to median isophotal levels of 27.1, 26.4, 26.4, and 25.4 mag arcsec⁻² in g' , r' , i' , and z' , respectively. In order to run the program in "dual image mode", it was necessary to align the images. Thus, because of rotations and shifts, parts of the images near the borders were lost.

Positions and magnitudes (total and aperture) were obtained for all objects present in all bands for each pair. We adopted 3 arcsec aperture magnitudes, m_{ap} , to measure colors. Aperture magnitudes were also obtained to compare our data with others in the literature. For the total magnitude of an object, we have adopted a color corrected isophotal magnitude. For example, if the objects were detected in the g' band, then $g' = g_{iso}$, $r' = g_{iso} - (g_{ap} - r_{ap})$, etc., where m_{iso} is the isophotal magnitude given by SExtractor. After measuring the magnitudes they were corrected for Galaxy extinction, with the absorption coefficients A_λ obtained from Schlegel et al. (1998) using NED and interpolated to GMOS bands.

We have used the class-star parameter of SExtractor, which ranges from 0 (galaxies) to 1 (stars), to separate stars from galaxies. Figure 1 shows this parameter versus the i' magnitude for the pair QP0110-0219. The star symbol in the plot represents all objects with $\text{FWHM} \leq \text{seeing}$. If we consider all objects with class-star < 0.8 as galaxies, a threshold often adopted in the literature (e.g. Kodama et al. 2004; Caputi et al. 2006), we find that 2 % of the objects with $\text{FWHM} \leq \text{seeing}$ have class-star < 0.8 and that 7 % of the objects with $\text{FWHM} > \text{seeing}$ have class-star ≥ 0.8 . On the other hand, if we adopt a threshold of 0.9, we have a similar contamination (~ 2 %) of the galaxy sample and only 4 % of the objects with $\text{FWHM} > \text{seeing}$ have now class-star ≥ 0.9 . The results for the other fields are similar. We then decided to adopt the class-star value of 0.9 to separate stars from galaxies. The same criteria was adopted by Capak et al. (2004) to determine number counts in the HHDFN.

In order to estimate the completeness magnitude of the observations, we have plotted the logarithmic number of detected objects as a function of the total magnitude in the band used for detection. From visual inspection of the turnover magnitudes, we estimated that the observations are complete down to $i' = 24$ for QP1310+0007 and QP0110-0219, $g' = 25$

for QP1355-0032, and $g' = 24.5$ for QP0114-3140.

It is interesting to know how the magnitudes above compare with those of a M^* -galaxy at the redshift of the pairs. We have estimated the value M^* in two ways, as follows. Ellis & Jones (2004) obtained $K^* \sim 18$ for clusters of galaxies with redshifts between 0.8 and 1.0. Considering the value for $(I - K) \sim 2.9$ obtained by Stanford et al. (2002) for the cluster 3C 184 ($z = 0.996$), we have $I^* \sim 20.9$. On the other hand, using spectrophotometric synthesis models, Fukugita et al. (1995) obtained $(i' - I_c) \sim 0.7$ for galaxies at $z = 0.8$. Then, we obtain $i'^* \sim 21.6$. In the second case, we may consider the Coma cluster as representative of a $z = 0$ cluster. Mobasher et al. (2003) studied its luminosity function and found $M_R^* \sim -21.79 + 5 \log h_{65}$. For galaxies at $z = 0$, Fukugita et al. (1995) obtained $(r' - R_c) \sim 0.22$ and $(r' - i') \sim 0.30$, therefore $M_{i'}^* \sim -21.71$ for the cosmology adopted here. We have calculated i'^* with

$$m = M(z = 0) + 5 \log d_L [Mpc] + 25 + k(z) + e(z) \quad (1)$$

where d_L is the luminosity distance, $k(z)$ is the k-correction and $e(z)$ is the evolution correction. In the cosmology adopted here, $d_L \sim 6000 Mpc$ at $z \sim 1$. Using $k(z)$ and $e(z)$ values published by Fukugita et al. (1995) and Poggianti (1997) respectively ($k_{i'} \sim 0.9$ and $e_{i'} \sim -1.3$) and the value obtained to $M_{i'}^*$ at $z = 0$, we obtain $i'^* \sim 21.8$. Considering the uncertainties of the approaches, the agreement of the two values is very good. We have then adopted the mean value $i'^* \sim 21.7$. This value is similar to that obtained by Blakeslee et al. (2006) ($i_{775}^* = 22.0 \pm 0.1$ AB) for early-type galaxies at $z = 0.83$. This result shows that the completeness magnitude of our fields corresponds to $\sim M^* + 2$ at the redshift of the pairs.

3.1. Comparison with HHDFN and ACS-GOODS photometry

Our approach to compute photometric redshifts (§4) makes use of a training set with galaxies of known redshifts measured in the same photometric bands. Consequently, photometric redshifts are very sensitive to small zero-point changes. In order to examine this point, we have made a comparison between our photometry with those available for the HHDFN (Hawaii Hubble Deep Field North) region (Capak et al. 2004) and for the ACS-GOODS (Advanced Camera for Surveys - Great Observatories Origins Deep Survey) region (Cowie et al. 2004).

Although one region is contained in the other, the photometric and spectroscopic data available for them are different. A comparison with HHDFN is useful because it contains ACS-GOODS and has a photometric completeness similar to those of our fields. ACS-GOODS, on the other hand, has hundreds of measured spectroscopic redshifts and will be

adopted as the training set for our photometric redshift method. Since the photometry of these fields (in $UBVRIZ'$) is different of our photometry (in $g'r'i'z'$), they were interpolated to the GMOS bands adopted here.

First we have considered the HHDFN region which has photometry complete down to $R = 24.5$. We compared the photometric distribution of galaxies in our fields within the magnitude completeness limit of each band with the corresponding distributions using the interpolated magnitudes. We estimated the shift that is required in the zero-point of our photometric bands so that the median of the magnitude distribution (for galaxies brighter than the completeness limit) of HHDFN and ours match each other. We have used an iterative algorithm, adding to our magnitudes a shift obtained in each step until convergence. The median of the absolute value of the shifts is 0.07.

Many are the possible sources of these shifts. A possibility is the magnitude interpolation required in this approach. Another one is cosmic variance, since the galaxy catalogues considered here are not large enough. Indeed, a photometric study with SDSS data made by Fukugita et al. (2004) shows that, besides Galaxy extinction, the principal cause for variations in number counts is the large-scale clustering of galaxies. This dispersion increases for smaller areas, being greater than 0.2 magnitudes for areas smaller than 0.01 deg^2 , as is our case.

After applying the zero-point shifts in our magnitudes, we compared our galaxy number counts with those from the ACS-GOODS data in 0.5 mag intervals for objects brighter than the apperture magnitude $z' = 22$. It can be verified that, for all fields, we obtain a good match between our number counts and those of ACS-GOODS.

4. Photometric redshift analysis

Determining the redshifts of the galaxies in our fields allows us to separate the galaxies belonging to a possible cluster or group at the redshift of the pair from the foreground and/or background galaxies. Here we adopt photometric redshifts for this task.

Photometric redshift estimation is often done by comparing the magnitudes of an object with the magnitudes of templates obtained with spectrophotometric evolution models, as is the case of Zpeg (Le Borgne et al. 2002) and HyperZ (Bolzonella et al. 2000). Here we adopt another approach: instead of a galaxy model, we use real data- magnitudes and spectroscopic redshifts- obtained in galaxy surveys. We compare the magnitudes of our galaxies with magnitudes in the same bands of real galaxies with known spectroscopic redshift to parametrize a local empirical relationship between magnitudes or colors with redshift.

This is done using a locally weighted regression algorithm (LWR) developed by our group (Santos et al. 2007, in preparation). The same type of data-driven approach is adopted in the ANNz photometric redshift package (Firth, Lahav & Somerville 2003), which applies instead artificial neural networks for this task.

4.1. Method

LWR is an algorithm designed to provide a continuous non-linear mapping between sets of variables (e.g., Atkeson, Moore & Schall 1997). Our LWR method is discussed in detail and compared with other methods in Santos et al. (2007, in prep.). Here we only outline its main characteristics. The method works with magnitudes or colors (and even with other galaxy properties, like diameter or type) but here we use colors.

The method works with two data sets: the training set (having known spectroscopic redshifts) and the test set (for which we want to calculate the redshift). Obviously, both sets must have the magnitudes and/or colors measured in the same bands and in the same photometric system.

LWR establishes a linear relationship between colors and redshifts that is local because the redshift estimation in a given point in color space weights more heavily the data points in the neighborhood of this point than those more distant. The training set contains colors and spectroscopic redshift for all objects. From these values we build a redshift estimator which will be applied to our galaxies, in the test set. We assume that the local relation between colors and redshifts is linear:

$$z(\mathbf{x}) = a_0 + \mathbf{a}^T \cdot \mathbf{x} = a_0 + \sum_{i=1}^n a_i x_i \quad (2)$$

where \mathbf{x} is a vector containing the n colors of a given object, $z(\mathbf{x})$ is the redshift and T stands for transpose matrix. For each object in the test set, with colors in point \mathbf{x} , we determine the values of coefficients $a_0 \dots a_n$ and then the redshift by minimizing the weighted χ^2 function with the N objects of the training set:

$$\chi^2 = \sum_{j=1}^N \omega_j^2 (y_j - a_0 - \mathbf{a}^T \cdot \mathbf{x}_j)^2 \quad (3)$$

where ω_j is the weight associated to the j -th data point. The locality of the fitting is assured by adopting a weight function which decreases as the euclidean distance $d(\mathbf{x}, \mathbf{x}_j)$ between points \mathbf{x} and \mathbf{x}_j increases:

$$\omega_j = \exp \left(\frac{-d^2(\mathbf{x}, \mathbf{x}_j)}{2K^2} \right) \quad (4)$$

The K parameter is a kernel-width that determines the “effective volume” around point \mathbf{x} : only points within this sphere effectively affect the values of the parameters and the redshift estimate. This parameter was determined in this work by dividing randomly the training set objects in 2/3 for training (TS) and 1/3 for validation (VS). For galaxies in VS we computed z_{phot} with eq. 2 using galaxies in TS to obtain the coefficients. This procedure was then repeated one hundred times. For each realization of TS and VS, we compute the rms square deviation between z_{phot} and z_{spec} for the objects in VS, σ_z , and choose as optimal K the value for which σ_z is minimum.

It is worth mentioning that redshift estimates with the LWR method are heavily dependent on the training set adopted (besides, of course, the set of colors available). In particular, the redshift accuracy increases with the size of the training set and depends strongly on the homogeneity of the photometric calibration of the training and test sets.

4.2. Application to our sample

We adopt in this work the (interpolated) photometric data and spectroscopic redshifts of the ACS-GOODS region as our training set. Since the method allows using colors or magnitudes for photometric redshift estimation, we have used colors (but none of the results reported in the next section depend of this choice). Using magnitudes we would have to limit our sample at $z' = 22$ (the ACS-GOODS spectroscopic completeness), but our sample photometry goes deeper; it is complete at least down to $i' = 24$. When we use colors, such limit is not necessary and we are able to estimate photometric redshifts for fainter objects, even without spectroscopic data for $z' > 22$.

The value $K = 0.33$ was determined by the procedure described in the previous section as the median value of 100 simulations. The histogram in Figure 2 shows the redshift error distribution for all simulations. In what follows we consider the mean value, $\sigma_z = 0.16$, as the redshift error for the training set ACS-GOODS. Figure 2 also shows the comparison between z_{phot} and z_{spec} for the 1/3 of galaxies from ACS-GOODS used for validation corresponding to the simulation with this mean value.

Having obtained photometric redshifts for all fields containing quasar pairs, we may start looking for structures around the redshift of the pairs, that is, objects with $z_{phot} = z_{pair} \pm \Delta z$. We made experiments with Δz equal to 0.1, 0.16 and 0.2, obtaining similar results. Therefore we only present here results with $\Delta z = \sigma_z = 0.16$. For comparison, Toft et al. (2003), in a photometric study of the galaxy cluster MG2016+112 at $z = 1$, adopted $\Delta z = 0.25$. Note that the error σ_z should depend of the photometric errors, the number of colors, and the size

of the training set.

5. Results

We present in Figure 3 the galaxy redshift distribution in the field of each quasar pair. All fields show a peak in the interval $z \in [z_{pair} - \sigma_z, z_{pair} + \sigma_z]$. We now analyse some properties of the galaxy distribution in this redshift interval aiming at constraining the nature of the environment inhabited by the quasar pairs of our sample.

5.1. Galaxy overdensities

We must know the expected number of galaxies in this interval, to verify the significance of the galaxy excess around z_{pair} . For this estimate we have assumed that the HHDFN region is representative of the overall galaxy distribution. This sample is appropriate for this analysis because its photometric depth is comparable to that of our fields. Photometric redshifts were obtained with the method discussed in the previous section. We then defined the galaxy overdensity in the interval $z_{pair} \pm \sigma_z$ as

$$\delta = \frac{n_{pair} - n_H}{n_H} \quad (5)$$

where n_{pair} and n_H are the number densities of galaxies in this redshift interval for a given field and for the HHDFN, respectively. We have considered as galaxies in HHDFN all objects with $z_{phot} > 0$.

Values of δ for each pair are shown in Table 3. Errors in δ were determined assuming Poissonian errors for N_{pair} and N_H . The overdensity δ ranges from 0.6 to 1.6 and is significant in all cases. Note that these results are affected by cosmic variance, since we have used only one reference field and the area occupied by HHDFN (0.2 square degrees) is very small, so that n_H is affected by the galaxy clustering in the HHDFN region. We have arrived at similar results using the VIMOS VLT Deep Survey around the Chandra Deep Field South (Le Fèvre et al. 2004) and the Gemini Deep Deep Survey (Abraham et al. 2004) regions.

5.2. Distribution of galaxies

In order to investigate the clustering properties of the galaxies in the chosen redshift interval around a quasar pair, we calculated the median projected distance between galaxies

and compared them with the same quantities obtained with 1000 simulations of random uniform galaxy distributions with the same number of objects and the same projected area of the observed fields. We may then define a confidence level, CL , that a field presents a galaxy distribution more clustered than an uniform distribution:

$$CL = \frac{N(\Delta\theta > \Delta\theta_f)}{N_s} \quad (6)$$

where $N(\Delta\theta > \Delta\theta_f)$ is the number of simulated fields with median projected distances larger than that of the observed fields and N_s is the total number of simulations.

We summarize the results of this analysis in Table 3. Two pairs are strongly clustered (QP1355-0032, QP0110-0219), one is moderately clustered (QP1310+0007) and one (QP0114-3140) is not clustered at all.

5.3. Richness

In order to estimate the richness of our fields, we have adopted an approach similar to the traditional Abell’s richness criterion (Abell 1958), defined as the number of galaxies brighter than $m_3 + 2$ (where m_3 is the magnitude of the third brightest cluster member) within a radius of $1.5 h_{100}^{-1}$ Mpc of the cluster center. A cluster is considered rich if it contains more than 30 galaxies according to such a definition.

The Abell’s radius considering the cosmological model adopted here is 2.1 Mpc. Assuming that the brightest galaxy in the redshift interval $z_{pair} \pm \sigma_z$ is the brightest cluster galaxy, we computed the number of galaxies brighter than $i'_3 + 2$ by scaling their number in each field to the Abell area ($N^{esc} = N/\Sigma$, where $\Sigma = A_{par}/A_{Abell} \sim 0.5$). This result was corrected for contamination due to background/foreground objects using counts in the HHDFN region. The results are shown in Table 3. All but one of the putative clusters are rich, according with this criterion. The field of QP1310+0007 seems to be the poorest of our four fields, and is poor also with Abell’s criterion. However, this is the pair with the brightest galaxy in the corresponding redshift interval among all quasar pairs, and its poorness may be an effect of galaxy counts, since they grow strongly for increasing magnitude. Furthermore, note that our fields are smaller than the Abell’s radius, then the quasars could be in a poor cluster, group, or in the neighborhood of a cluster. On the other hand, the pair QP0114-3140, which is not rich by the results of Sections 5.1 and 5.2, has $R=0$ in Abell’s classification. It is, then, appropriate to look for other richness estimators to confirm or not these results.

Another useful richness indicator is the number of bright galaxies, assumed here as those

brighter than $i'^* + 1$ present in the field. This number is estimated for galaxies in the pair redshift interval and is corrected with the corresponding HHDFN counts (scaled to the field area). The results are also presented in Table 3. All fields seems to contain a considerable number of bright galaxies.

It is interesting to compare our results with those obtained by Postman et al. (2002). These authors studied a variety of Abell-like richness indicators in an I-band cluster survey. One of these indicators, $N_{A,0.5}$, is defined as the number of galaxies with magnitude between m_3 and $m_3 + 2$ within a radius of $666 h_{75}^{-1} kpc$. They show that this indicator is related to Abell's richness, N_A , as $N_{A,0.5} \sim 0.44 N_A$. We have used this relation to estimate Abell's richness from $N_{A,0.5}$. For 31 clusters with redshifts between 0.9 and 1.0, we obtain $N_A = 54$ galaxies. That means that fields have a richness $R \sim 1$, which may be compared with the numbers present in Table 3: only QP1310+0007 seems poorer than the clusters at comparable redshift studied by Postman et al. (2002).

5.4. The red sequence

The red sequence is a characteristic of the color-magnitude diagrams of early-type galaxies of groups and clusters. In a color-magnitude diagram these galaxies have very similar colors following a linear relation and their integrated colors are progressively bluer for weaker magnitudes. This relation is also known as color-magnitude relation (CMR).

We have examined the red sequence in the $(i' - z') \times i'$ diagram of galaxies in the redshift interval of each pair. The use of the color $(i' - z')$ is based on its capability to identify early-type galaxies, since at $z \sim 1$ the 4000 Å break lies in the i' band and consequently the early-type galaxy color $(i' - z')$ are very red. The fields around quasar pairs QP1310+0007 and QP0110-0219 (Figures 4 and 6 - top-right) present a peak in the color distribution at $0.6 \leq i' - z' \leq 1.0$. Comparing our data with a similar distribution for HHDFN, we verify that these peaks represent an excess of 1.7σ and 3.3σ , respectively. Therefore, in this interval, we would expect to find a red sequence in the color-magnitude diagram. Indeed, for QP0110-0219 we note clearly that the galaxies form a red sequence in $i' - z' \sim 0.8$ (Figure 6 - top-left), the value obtained by Tanaka et al. (2006) in spectroscopically confirmed structures at $z \sim 0.9$. Besides, if we consider the projected distribution of these red-sequence galaxies (Figure 6 - bottom), we notice that they have a filamentary-like distribution similar to what is observed in other $z \sim 1$ clusters, and considered typical of clusters in process of formation (e.g., Toft et al. 2003).

The red galaxies of QP1310+0007 present a broad distribution in the color-magnitude

diagram (Figure 4 - top-left). They also present a clump-like projected distribution (Figure 4 - bottom). The other two fields have less-significant red sequences (Figures 5 and 7). The cluster CL1604+4321, at $z \sim 0.9$, the less massive of the clusters studied by Homeier et al. (2006), presents a lack of bright elliptical galaxies ($\sim M^*$). The authors suggest that this cluster has not yet had time to complete the red sequence. This may be also the case for the structures associated to QP1355-0032 and QP0114-3140.

5.5. Properties of the fields around quasar pairs

The properties of the environment associated with each quasar pair are summarized in Table 4. We now discuss each pair individually.

5.5.1. QP1310+0007

This quasar pair is formed by J131046+0006 (a radio-quiet object) and J131055+0008 (a radio-loud quasar) at redshifts 0.925 and 0.933, respectively. They have an angular separation of 177 arcsec, corresponding to 1.4 Mpc in the adopted cosmology. Its density contrast is the smallest among all quasar pairs. However, the galaxy distribution analysis shows that the galaxies in this field are clustered at some degree, i.e., the median projected distance between galaxies is smaller than in a random uniform field in 67 % of the simulations. This field has been classified as poor with the Abell’s criterion, and we have found 20 galaxies with magnitude $i' < i'^* + 1$. The galaxy color distribution shows a prominent peak in $0.6 \leq i' - z' \leq 1.0$, corresponding to the red sequence. The red galaxies present a clumpy distribution, but without central condensation. The presence of a significant amount of early-type galaxies plus the relative poorness of this field indicate that this can be the seed of a structure that can become a rich galaxy cluster at $z = 0$.

5.5.2. QP1355-0032

J135457-0034 and J135504-0030 constitute this pair; the first is radio-loud and the second is radio-quiet. The projected separation between them is 252 arcsec, or 2.0 Mpc, with redshifts 0.932 and 0.934, respectively. The redshift interval $z_{pair} \pm \sigma_z$ shows the largest galaxy excess among all quasar pairs discussed in this work. The median projected distance between galaxies resulted smaller than in a random uniform field in 98.5 % of the cases, meaning that these galaxies are strongly clustered. This is the richest field in our sample

accordingly to Abell’s criterion and also the one with the largest number of bright galaxies ($i' < i'^* + 1$), however its red sequence is modest and the red galaxies do not present a clustered distribution. Its richness and number of bright galaxies are the major indications that this quasar pair is probably in a galaxy cluster.

5.5.3. *QP0110-0219*

This quasar pair is formed by a radio-loud quasar (Q 0107-0235) and a radio-quiet quasar (PB 6291) at redshifts 0.958 and 0.956, respectively. The angular separation of 77 arcsec (0.6 Mpc) is the smallest of the sample. The overdensity in the redshift interval is significant as for the other pairs. The galaxy distribution is the most clustered of all samples, accordingly to the CL values in Table 3. The field is rich by Abell’s criterion, but presents only 12 bright galaxies. The red sequence is clearly present in the color-magnitude diagram at $i' - z' \sim 0.8$. The red galaxies present a filamentary-like distribution and there is a galaxy excess around the radio-loud quasar. These results indicate that QP0110-0219 is indeed a rich cluster.

Moreover, we have verified that QP0110-0219 has been serendipitously detected (but unreported) in X-ray with a pointed *ROSAT* PSPC observation of 6.6 ks. We have estimated the bolometric X-ray luminosity assuming that all detected flux (background corrected) comes from the ICM: $L_{X,\text{bol}} \sim 5 \times 10^{45} \text{ ergs s}^{-1}$. Such luminosity is well above a typical cluster X-ray luminosity and may be contaminated by the X-ray emission from one or both quasars. On the other hand, the typical quasar X-ray luminosity [2–10 keV] is around $10^{44} \text{ erg s}^{-1}$, thus the quasars in the pair may not account for all X-ray emission. Besides, the total emission [0.5–8.0 keV] within 3 arcmin is about 10 times higher than the typical quasar emission in this band; therefore the observed X-ray flux is consistent with emission from quasars and a possible cluster around them. This is the single pair in our sample detected in X-rays so far. The other fields were not detected in the Rosat All Sky Survey, nor in the pointed observations.

5.5.4. *QP0114-3140*

This pair is formed by radio-quiet quasars. J011441-3139 has $z = 0.974$ and J011446-3141 has $z = 0.968$. The separation between them is 144 arcsec (1.1 Mpc). This field shows a significant overdensity, no clustering, and no red sequence. It also seems rich with Abell’s criterion and has a comparatively large number of bright galaxies. The evidence for the

presence of a rich cluster at the redshift of the quasar pair is not as compelling in this case, compared with the other 3 pairs.

6. Summary

We have studied the environment traced by quasar pairs at $z \sim 1$, using images in g' , r' , i' , and z' bands obtained with GMOS at Gemini North and South. In order to identify galaxies in a redshift interval close to that of the quasar pairs, we have estimated photometric redshifts with the LWR method, using ACS-GOODS data as a training set. The rms dispersion of the difference between our photometric redshift and the spectroscopic redshift in the training set is $\sigma_z = 0.16$. We have adopted the interval $z = z_{pair} \pm \sigma_z$ for the analysis of the pair environment.

When compared with the HHDFN region, all fields show a significant overdensity in the redshift interval of the pair. In all cases this excess is larger than 3.5σ .

We investigated the clustering of the galaxies near the pair by estimating a confidence level, CL , that the galaxies are more concentrated than in a uniform distribution. We have also estimated the richness of each redshift interval with a variant of Abell’s criterion, as well as by the number of bright galaxies. We verified whether a red sequence is present and the form of the projected distribution of red galaxies.

The analysis indicates that probably three out of our four quasar pairs are members of galaxy clusters. For one of the pairs we did not find strong evidence for it: QP0114-3140 could be in a poor cluster, group, or in the neighborhood of a cluster, since our fields are lesser than Abell’s radius. Taken at face value, this result shows that quasar pairs are indeed good tracers of the large scale structure at high z . However, with only four quasar pairs in our sample we are not able to say at what level targeting a quasar pair increases the probability of finding a rich galaxy cluster as compared to targeting a single quasar. A study of larger and homogeneous samples would be necessary to clarify this point. An extension of our work to other redshifts may be also useful and may provide interesting clues on the evolution of large-scale structure and galaxy clustering.

This work is based on observations obtained at the Gemini Observatory, which is operated by the Association of Universities for Research in Astronomy, Inc., under a cooperative agreement with the NSF on behalf of the Gemini partnership: the National Science Foundation (United States), the Particle Physics and Astronomy Research Council (United Kingdom), the National Research Council (Canada), CONICYT (Chile), the Australian Research

Council (Australia), CNPq (Brazil) and CONICET (Argentina).

We would like to thank the Gemini staff for obtaining the observations in queue mode. We also thank G. B. Lima Neto for many useful discussions, and the anonymous referee, whose comments helped to improve this paper. We are grateful for the support provided by the Brazilian agencies CNPq and FAPESP. We made use of the NASA/IPAC Extragalactic Database, which is operated by the Jet Propulsion Laboratory, California Institute of Technology, under contract with NASA.

REFERENCES

- Abell, G. O., 1958, *ApJS*, 3, 211
- Abraham, R. G., Glazebrook, K., et al., 2004, *AJ*, 127, 2455
- Atkeson, C. G., Moor, A. W. & Schaal, S. A., 1997, *Locally Weighted Learning. AI Review*, 11, 11
- Bekki, K., 1998, *ApJ*, 502L, 133
- Bertin, E. & Arnouts, S., 1996, *A&AS*, 117, 393
- Blakeslee, J., et al., 2006, *ApJ*, 644, 30
- Bolzonella, M., Miralles, J. & Pelló, R., 2000, *A&A*, 363, 476
- Butcher, H. & Oemler, A., 1984, *ApJ*, 285, 496
- Capak, P., et al., 2004, *AJ*, 127, 180
- Caputi, K. I., McLure, R. J., Dunlop, J. S., Cirasuolo, M. & Schael, A. M., 2006, *MNRAS*, 366, 609
- Clowes, R. G., & Campusano, L. E. 1991, *MNRAS*, 249, 218
- Clowes, R. G., & Campusano, L. E. 1994, *MNRAS*, 266, 317
- Coil, A. L., Hennawi, J. F., Newman, J. A., Cooper, M. C. & Davis, M., 2007, *ApJ*, 654, 115
- Cowie, L. L., Barger, A. J., Hu, E. M., Capak, P. & Songaila, A., 2004, *AJ*, 127, 3137
- Coldwell, G. V., Martínez, H. J. & Lambas, D. G., 2002, *MNRAS*, 336, 207

- Croom, S., Smith, R., Boyle, B., Shanks, T., Miller, L., Outram, P. & Loaring, N., 2004, MNRAS, 349, 1397
- Djorgovski, S., Stern, D., Mahabal, A. & Brunner, R., 2003, ApJ, 596, 67
- Ellis, S. C. & Jones, L. R., 2004, MNRAS, 348, 165
- Firth, A.E., Lahav, O., Somerville, R. S., 2003, MNRAS, 339, 1195
- Fukugita, M., Shimasaku, K. & Ichikawa, T., 1995, PASP, 107, 945
- Fukugita, M., Ichikawa, T., Gunn, J. E., Doi, M., Shimasaku, K. & Schneider, D. P., 1996, AJ, 111, 174
- Fukugita, M., Yasuda, N., Brinkmann, J., Gunn, J., Ivezić, Z., Knapp, G., Lupton, R. & Schneider, D. P., 2004, AJ, 127, 3155
- Gladders, M. D. & Yee, H. K. C., 2005, ApJS, 157, 1
- Haines, C. P., Clowes, R. G., Campusano, L. E. & Adamson, A. J., 2001, MNRAS, 323, 688
- Hall, P. B., & Green, R. F. 1998, ApJ, 507, 558
- Homeier, N., et al., 2006, ApJ, 647, 256
- Kaiser, N. 1984, ApJ, 284L, 9
- Kodama, T., Arimoto, N., Barger, A. & Aragon-Salamanca, A., 1998, A&A, 334, 99
- Kodama, T., Yamada, T., et al., 2004, MNRAS, 350, 1005
- Landolt, 1992, A. U., AJ, 104, 340
- Le Borgne, D. & Rocca-Volmerange, B., 2002, A&A, 386, 446
- Le Fèvre, O., Vettolani, G., et al., 2004, A&A, 428, 1043
- Mei, S., et al., 2006, ApJ, 639, 81
- Mobasher, B., Colles, M., Carter, D., Poggianti, B., Bridges, T., Kranz, K., Komiyama, Y., Kashikawa, N., Yagi, M. & Okamura, S., 2003, ApJ, 587, 605
- Mullis, C. R., Henry, J. P., Gioia, I. M., Böhringer, H., Briel, U. G., Voges, W., & Huchra, J. P. 2004, ApJ, 617, 192
- Poggianti, B., 1997, A&AS, 122, 399

- Postman, M., Lauer, T., Oegerle, W. & Donahue, M., 2002, *ApJ*, 579, 93
- Romer, A. K., Viana, P. T. P., Liddle, A. R., & Mann, R. G. 2001, *ApJ*, 547, 594
- Sánchez, S. & González-Serrano, J., 2002, *A&A*, 396, 773
- Schlegel, D. J., Finkbeiner, D. P. & Davis, M., 1998, *ApJ*, 500, 525.
- Söchting, I. K., Clowes, R. G., & Campusano, L. E. 2002, *MNRAS*, 331, 569
- Stanford, S. A., Eisenhardt, P. R., Dickinson, M., Holden, B. P. & De Propris, R., 2002, *ApJS*, 142, 153
- Surdej, J., Arp, H., Gosset, E., Kruszewski, A., Robertson, J. G., Shaver, P. A. & Swings, J. P., 1986, *A&A*, 161, 209
- Tanaka, I., Yamada, T., Turner, E. L., & Suto, Y., 2001, *ApJ*, 547, 521
- Tanaka, M., Kodama, T., Arimoto, N. & Tanaka, I., 2006, *MNRAS*, 365, 1392
- Toft, S., Soucail, G. & Hjorth, J., 2003, *MNRAS*, 344, 337
- van Dokkum, P., 2005, *AJ*, 130, 2647
- Véron-Cetty, M. P. & Véron, P., 2001, *A&A*, 374, 92
- White, S. & Frenk, C., 1991, *ApJ*, 379, 52
- Wold, M., Lacy, M., Lilje, P. & Serjeant, S., 2000, *MNRAS*, 316, 267
- Wold, M., Lacy, M., Lilje, P. & Serjeant, S., 2001, *MNRAS*, 323, 231
- Zhdanov, V. I. & Surdej, J. 2001, *A&A*, 372, 1

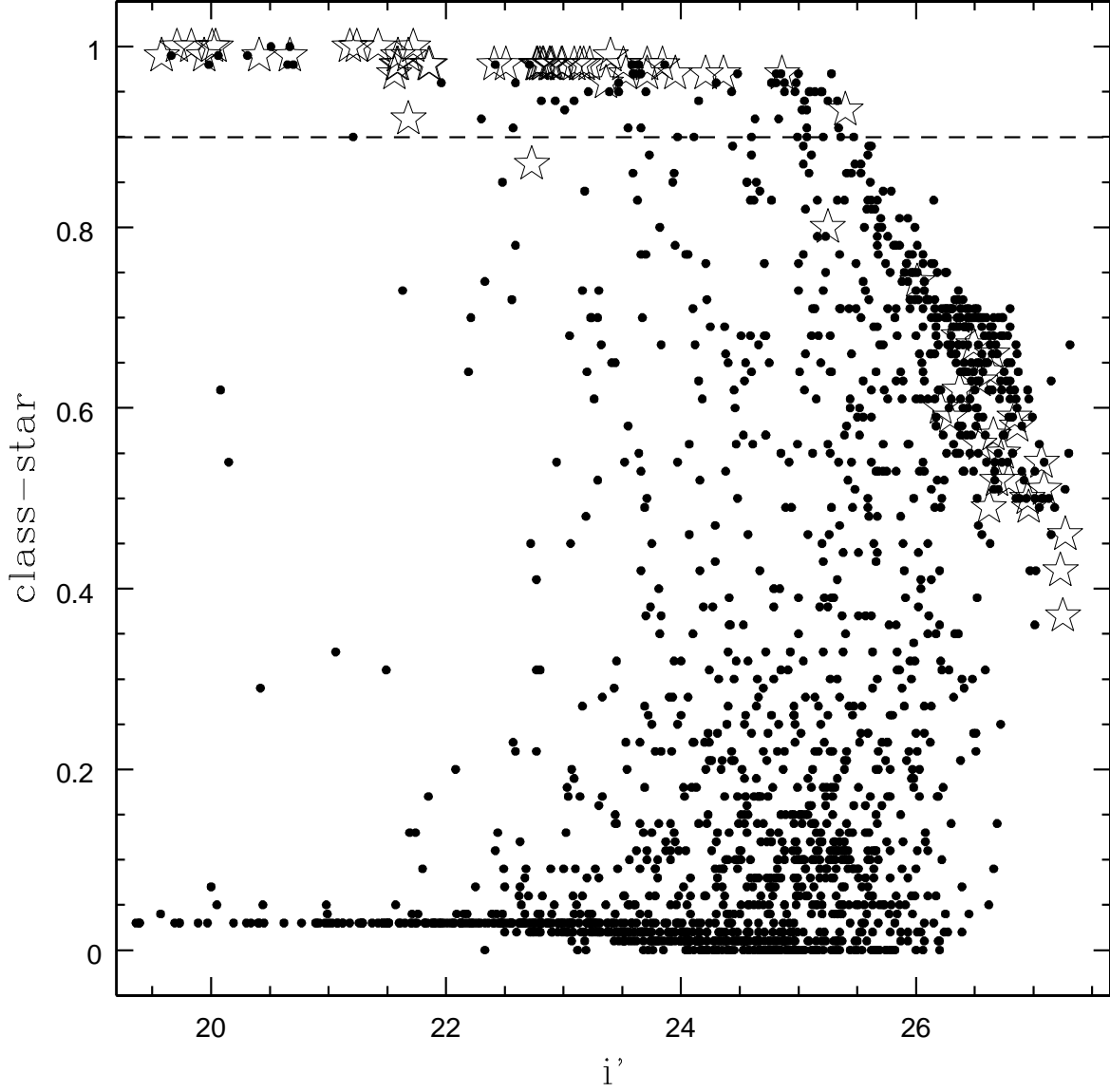


Fig. 1.— Star/Galaxy separation for the pair QP0110-0219. Stars represent objects with $\text{FWHM} \leq \text{seeing}$ and filled circles represent objects with $\text{FWHM} > \text{seeing}$. We have considered as galaxies all objects with $\text{class-star} < 0.9$ (dashed line).

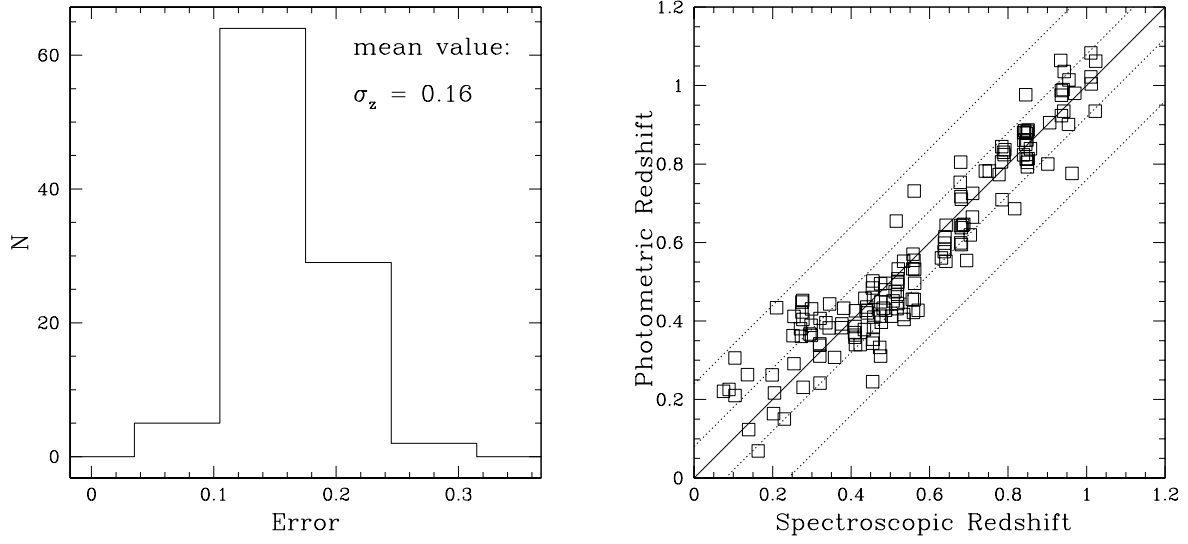


Fig. 2.— Left: photometric redshift error for 100 simulations. Right: comparison between photometric and spectroscopic redshifts for the 1/3 of galaxies from ACS-GOODS used for validation, corresponding to the simulation with photometric redshift error equal to $\sigma_z = 0.16$; the continuous line is the equality line and the dashed lines correspond to 1 and $3 \sigma_z$.

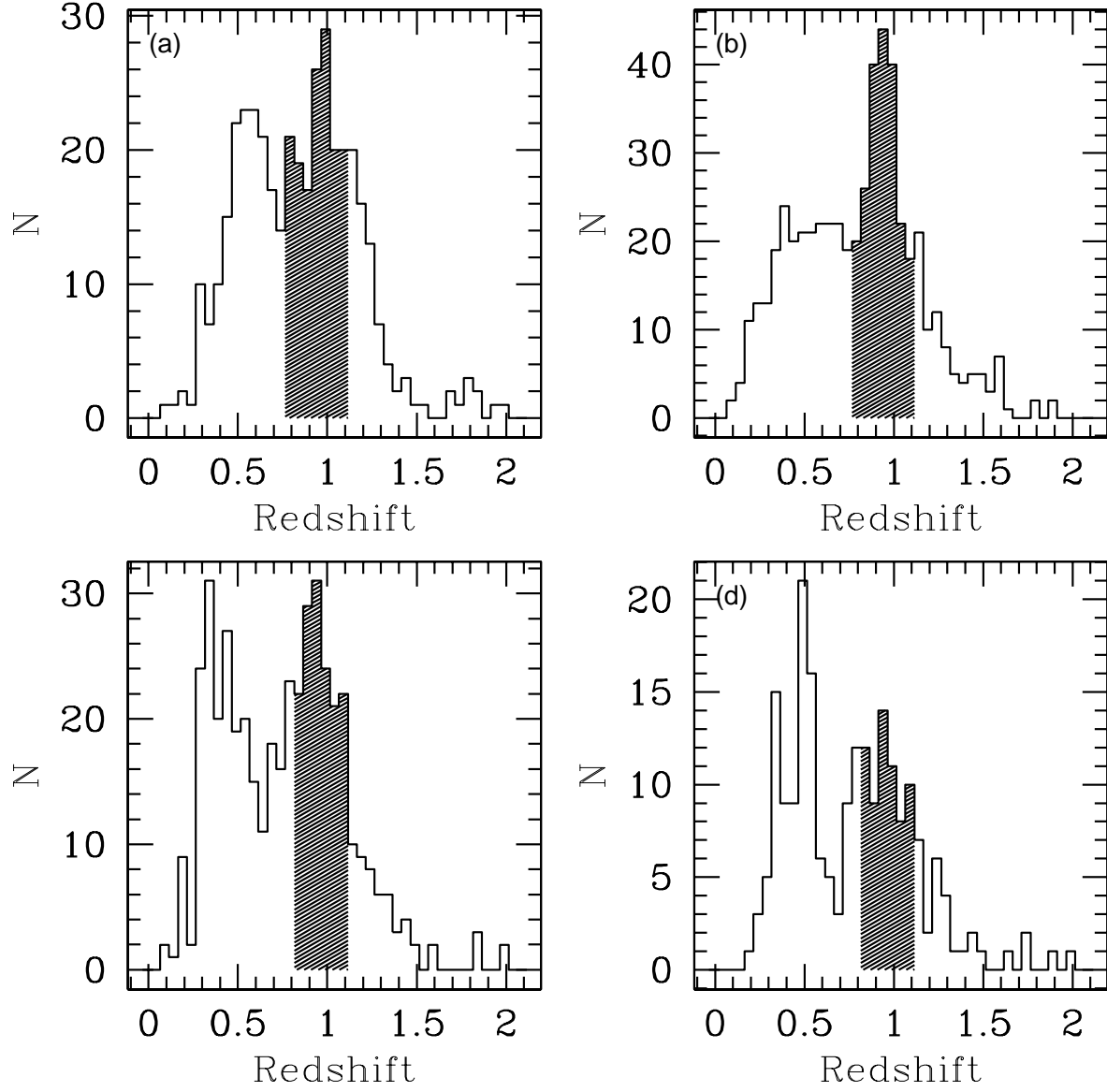


Fig. 3.— Distribution of photometric redshifts for each field containing a quasar pair: a) QP1310+0007, b) QP1355-0032, c) QP0110-0219, and d) QP0114-3140. The hatched area in each panel corresponds to $z_{pair} \pm \sigma_z$.

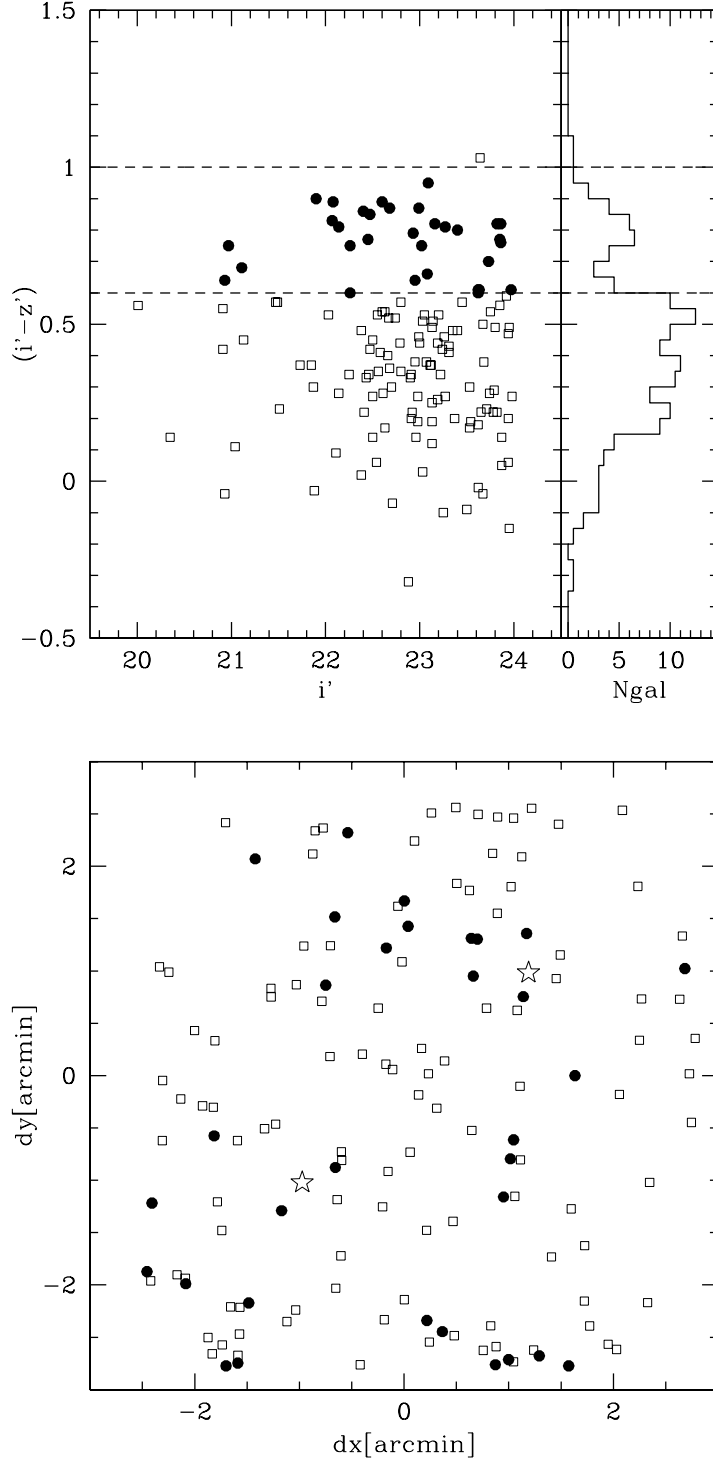


Fig. 4.— Results for the pair QP1310+0007. Galaxies within $z_{pair} \pm \sigma_z$. Top-left: color-magnitude diagram; galaxies in the red sequence are represented as filled circles. Top-right: histogram of the color distribution. Bottom: projected distribution of galaxies. The quasar pair is represented by stars and the galaxies in the red sequence as filled circles.

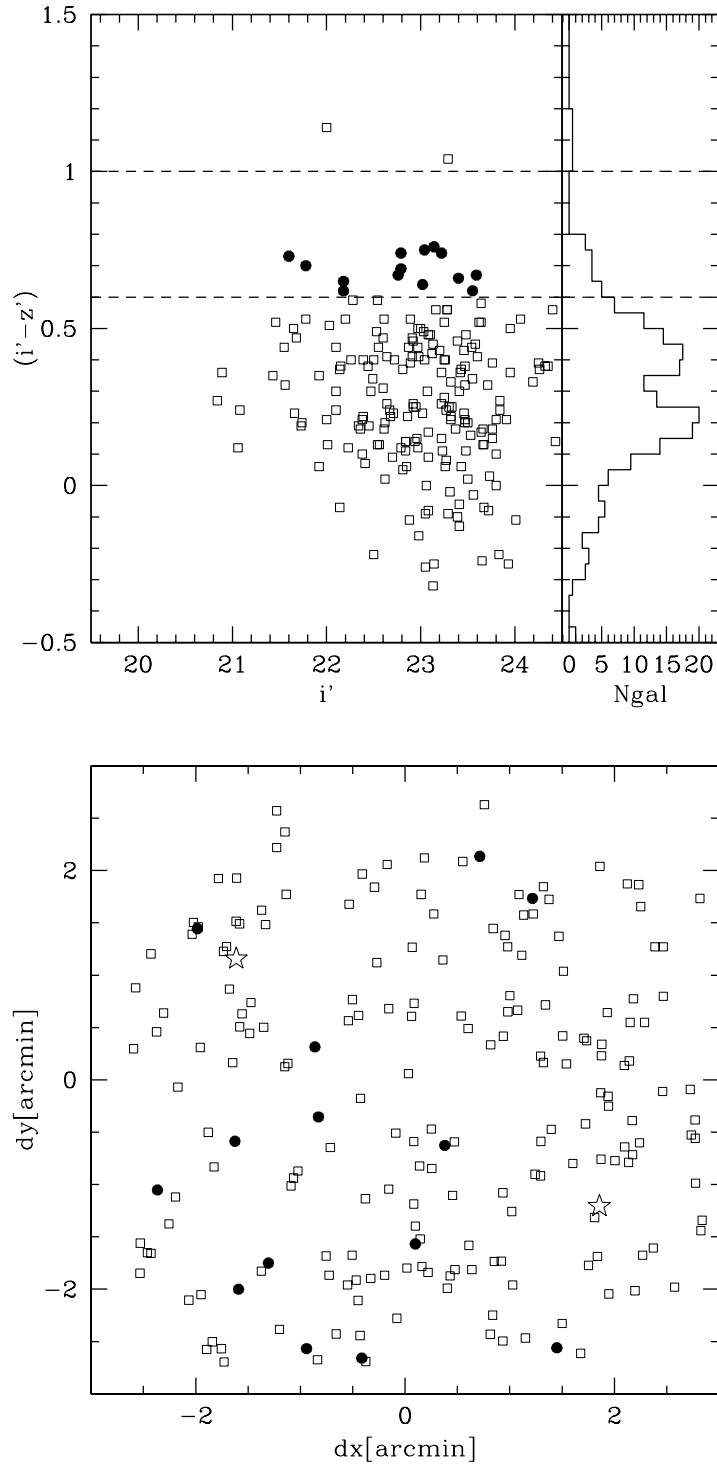


Fig. 5.— Same as Fig. 4 but for QP1355-0032.

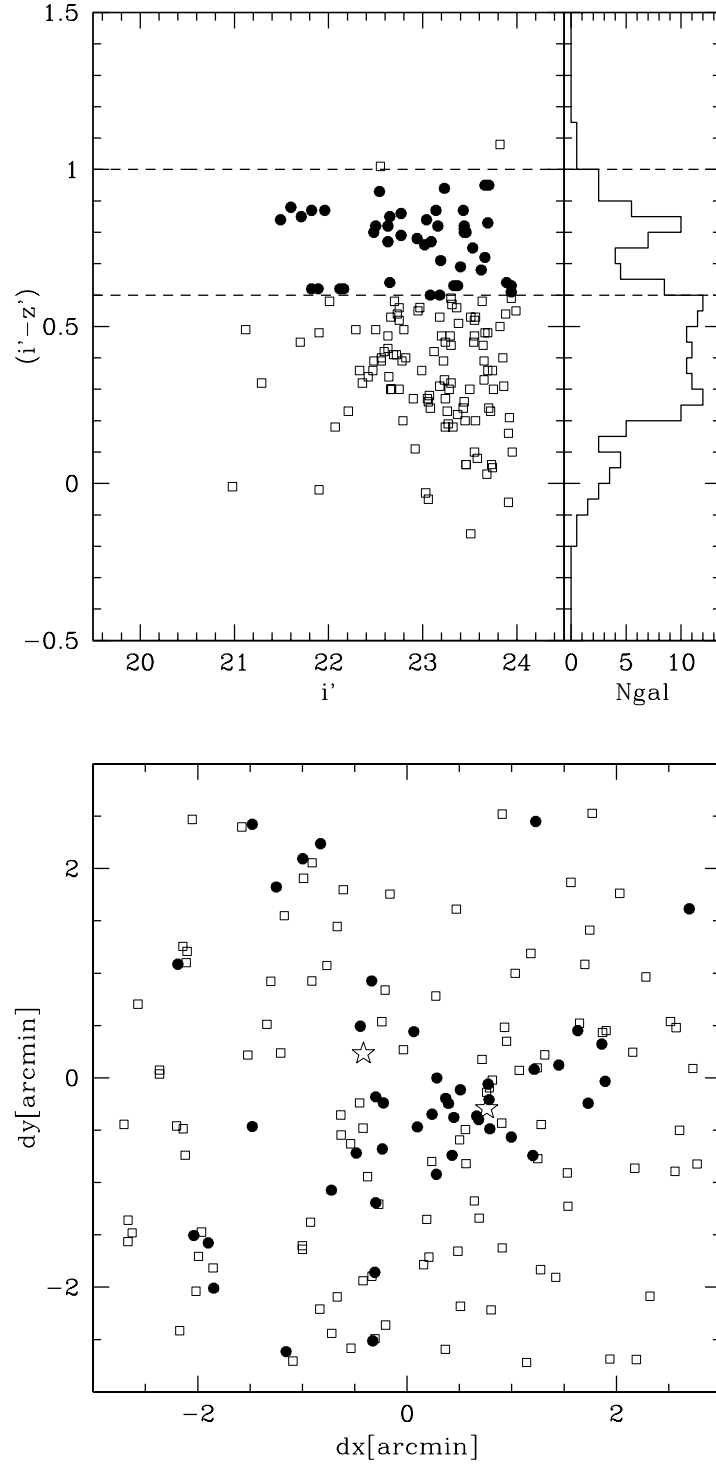


Fig. 6.— Same as Fig. 4 but for QP0110-0219.

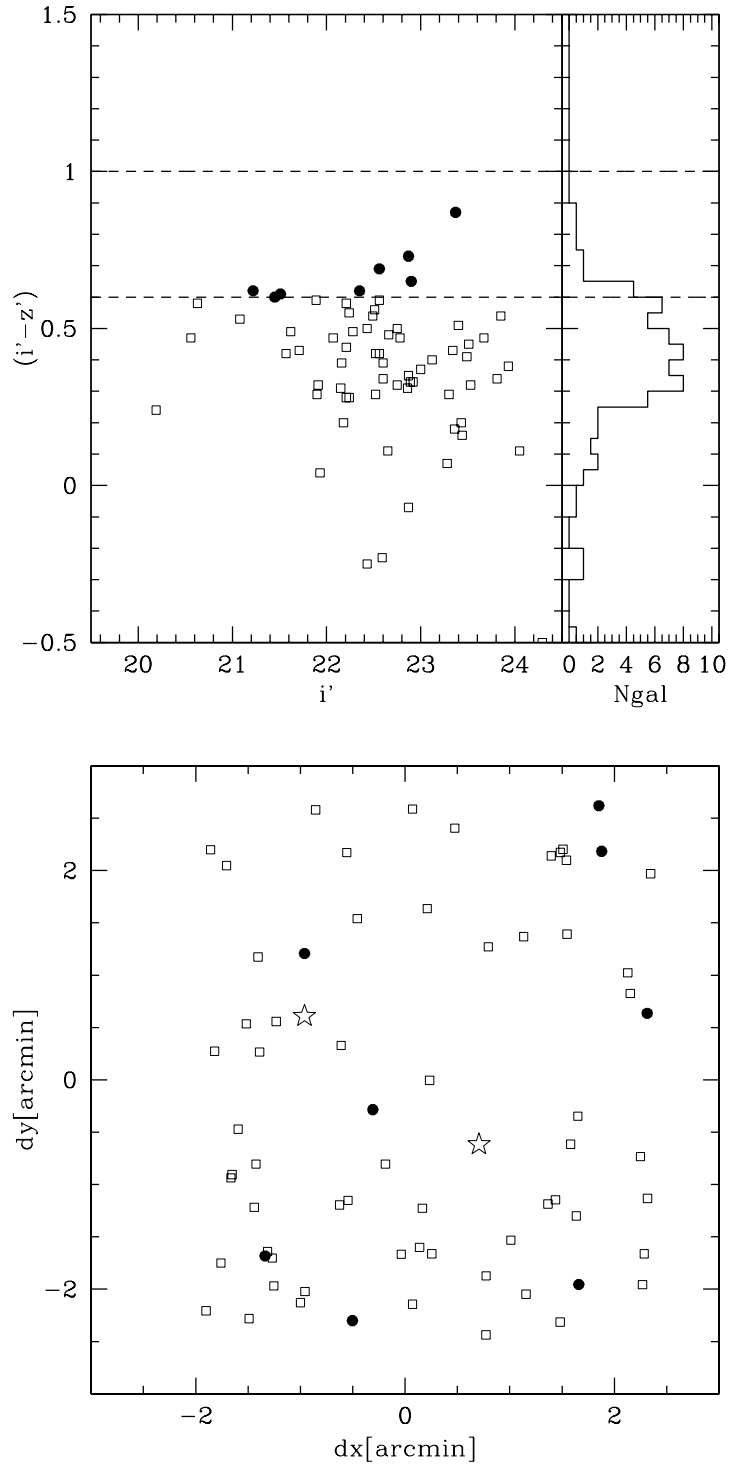


Fig. 7.— Same as Fig. 4 but for QP0114-3140.

Table 1. Sample Characteristics

Quasar Names	α (J2000)	δ (J2000)	z	$\Delta\theta$ (<i>arcsec</i>)	Quasar Pair Name
J131046+0006*	13 10 46.2	00 06 33	0.925	177	QP1310+0007
J131055+0008	13 10 55.9	00 08 14	0.933		
J135457-0034	13 54 57.2	-00 34 06	0.932	252	QP1355-0032
J135504-0030*	13 55 04.7	-00 30 20	0.934		
Q 0107-0235	01 10 13.2	-02 19 53	0.958	77	QP0110-0219
PB 6291*	01 10 16.3	-02 18 51	0.956		
J011441-3139*	01 14 41.8	-31 39 25	0.974	144	QP0114-3140
J011446-3141*	01 14 46.4	-31 41 31	0.968		

*Radio-quiet quasars

Table 2. Observations

Pair	Telescope	t_{exp} (seconds)				Identification Number
		g'	r'	i'	z'	
QP1310+0007	Gemini N	9×300.0	6×200.0	11×350.0	8×450.0	GN-2003A-Q-2/GN-2005A-Q-19
QP1355-0032	Gemini N	13×300.0	6×200.0	6×350.0	7×450.0	GN-2003A-Q-2/GN-2005A-Q-19
QP0110-0219	Gemini N	10×300.0	6×200.0	8×350.0	8×410.0	GN-2003B-Q-2/GN-2004B-Q-24
QP0114-3140	Gemini S	7×300.5	6×200.5	7×350.5	7×410.5	GS-2003B-Q-3/GS-2004B-Q-17

Table 3. Clustering Properties

Pair	δ	$\Delta\theta_{median}$ (arcmin)	CL_{median} (%)	i'_3	$N(i' < i'_3 + 2)$	$N^{esc}(i' < i'_3 + 2)$	$N(i' < i'^* + 1)$
QP1310+0007	0.58 ± 0.14	2.7	67.0	20.35	6 ($R < 0$)	13 ($R < 0$)	20
QP1355-0032	1.59 ± 0.19	2.6	98.5	21.06	95 ($R = 2$)	203 ($R = 4$)	58
QP0110-0219	0.70 ± 0.14	2.4	100.0	21.29	35 ($R = 0$)	72 ($R = 1$)	12
QP0114-3140	0.86 ± 0.23	2.8	0.5	20.63	34 ($R = 0$)	95 ($R = 2$)	36

Table 4. Summary of the quasar pair properties

Pair	δ	CL	N_A	RCM	C/F ^a	X-rays
QP1310+0007	ok	ok	x	ok	ok	–
QP1355-0032	ok	ok	ok	x	x	–
QP0110-0219	ok	ok	ok	ok	ok	ok
QP0114-3140	ok	x	ok	x	x	–

^aCluster-like or filament-like distribution.